# Conformational Changes of Bovine Serum Albumin Induced by Adsorption on Different Clay Surfaces: FTIR Analysis

S. Servagent-Noinville, M. Revault, H. Quiquampoix, M.-H Baron

# CONFORMATIONAL CHANGES OF BOVINE SERUM ALBUMIN INDUCED BY ADSORPTION ON DIFFERENT CLAY SURFACES: FTIR ANALYSIS.

S. Servagent-Noinville[1], M. Revault[1], H. Quiquampoix[2] and M-H Baron*[1]

[1]Laboratoire de Dynamique, Interactions et Réactivité, C.N.R.S-Université PARIS 6, UPR-1580, 2 rue Henry Dunant, 94320 Thiais, France; and [2]UFR de Science du Sol, INRA-ENSAM, 2 place Pierre Viala, 34060 Montpellier, France

*Abbreviated title:* Bovine Serum Albumin Adsorption on Talc and Montmorillonite.

***To whom the correspondence should be addressed.***

Dr M. H. Baron, Laboratoire de Dynamique, Interactions et Réactivité,

CNRS, 2 rue Henri Dunant, 94320-Thiais, France

Phone: 00 33 1 49 78 11 15

Fax: 00 33 1 49 78 13 23

*E-mail*: mh_baron@glvt-cnrs.fr

*Abstract*

Interactions between proteins and clays perturb biological activity in ecosystems, particularly soil extracellular enzyme activity. The pH dependence of hydrophobic, hydrophilic and electrostatic interactions on the adsorption of bovine serum albumin (BSA) is studied. BSA secondary structures and hydration are revealed from computation of the Amide I and II FTIR absorption profiles. The influence of ionization of Asp, Glu and His side chains on the adsorption processes is deduced from correlation between $p^2H$ dependent carboxylic/carboxylate ratio and Amide band profiles. We quantify $p^2H$ dependent internal and external structural unfolding for BSA adsorbed on montmorillonite, which is an electronegative phyllosilicate. Adsorption on talc, a hydrophobic surface, is less denaturing. The results emphasize the importance of electrostatic interactions in both adsorption processes. In the first case, charged side chains directly influence BSA adsorption that generate the structural transition. In the second case, the forces that attract hydrophobic side chains towards the protein-clay interface are large enough to distort peripheral amphiphilic helical domains. The resulting local unfolding displaces enough internal ionized side chains to prevent them establishing salt bridges as for BSA native structure in solution. On montmorillonite, a particular feature is a higher protonation of the Asp and Glu side chains of the adsorbed BSA than in solution, which decreases coulombic repulsion.

*Key words:* bovine serum albumin; conformational transition; protein adsorption; talc; montmorillonite; Fourier transform infrared spectroscopy.

# INTRODUCTION

Adsorption of proteins on solid surfaces plays a major role in biomedical, technological and environmental applications (1). The solid phase in soils has a large specific surface area and high adsorptive capacities for proteins (2-6). The interaction of enzymes with soil mineral surfaces modifies their catalytic activity (7-14) because of solvation and structural changes which occur upon adsorption (15). Electrostatic, hydrophobic, and hydrophilic interactions between proteins and mineral surfaces induce structural changes on the adsorbed proteins (16-24). The relative influences of these contributions on the degree of denaturation of the protein are not yet completely elucidated. In order to understand the weight of each interaction we have investigated the conformational changes of bovine serum albumin (BSA) on adsorption on two phillosilicates, montmorillonite and talc. The interesting property of these phyllosilicates is that they possess the same external chemical surfaces composed of siloxane groups, but differ in their surface electrical charge (25). Montmorillonite has an electronegative surface caused by isomorphic substitution occurring mainly in the alumina octahedral sheet while the basal surface of talc is hydrophobic with no electrical charges. Various spectroscopic techniques (NMR, fluorescence and circular dichroism) are currently used to study protein structural conformations in solution. FTIR-spectroscopy is best suited to compare secondary structures for proteins in solution, or adsorbed on a solid support (15, 21-24). In this way, we compared the conformational changes induced on BSA by adsorption, either on the hydrophobic and neutral talc, or on the electronegative montmorillonite. The influence of the pH on these structural modifications is analyzed in each case.

# MATERIALS AND METHODS

**Chemicals**

BSA (A-7638), obtained from Sigma, was used without further treatment. BSA is made up of 100 acidic side-chains with 41 Asp and 59 Glu residues and 99 basic side-chains with 23 Arg, 59 Lys and 17 His. The size of the crystalline protein should be that of an equilateral triangle with sides of 8 nm and depth of 3 nm, as for human serum albumin, HSA (26, 27). For BSA in solution, or adsorbed in suspension, the balance between negative and positive charges changes with pH. The isoelectric point (i.e.p.) is 4.8.

The clay-sized fraction ($< 2\mu$m) of a Wyoming montmorillonite, with a specific area of 800 m$^2$/g, was saturated with sodium, then dialyzed, to give a salt-free suspension as previously described (10). The surface is negatively charged with 1.25 10$^{-6}$ mol. m$^{-2}$. A talc from Luzenac, size fraction $< 10$ μm, with a surface area of 18.5 m$^2$/g and no surface electrical charge was used without preparation.

In order to shift the spectral absorption domain of water molecules bound to the polypeptide backbone of BSA out of the Amide I and II spectral range, all samples were prepared in $^2$H$_2$O medium (15, 21-24). A phosphate buffer (Na$^2$H$_2$PO$_4$) was used at final concentration 0.055 mol. L$^{-1}$ in $^2$H$_2$O. Several p$^2$H were obtained by adding $^2$HCl (28). Resulting solvents were added to solid protein and clay mixtures. The suspensions contained 4 g. L$^{-1}$ of BSA and 200 g. L$^{-1}$ of talc, or 30 g. L$^{-1}$ of BSA and 57 g. L$^{-1}$ of montmorillonite. Amounts of BSA are roughly in proportion to the specific area of the clays. The absence of protein in the supernatants after adsorption was checked by FTIR of the solution after centrifugation. Except for talc at p$^2$H $< 4.8$, spectra did not show any presence of BSA in the supernatant solutions. We noted that for p$^2$H $< 4.2$, buffers damaged the talc. For comparison

between adsorption on montmorillonite and talc only results obtained for $p^2H \geq 4.8$ are

discussed.


## Experimental


The FTIR-transmission spectra were recorded on a Perkin Elmer 1720

spectrometer equipped with a DTGS detector. Resolution was set at 4 cm$^{-1}$, using a

boxcar apodization. A Balston air-dryer (Whatman, UK) strongly reduced the water vapor

in the spectrometer during the measurements. Solutions of BSA in buffered $^2H_2O$ solutions

were inserted into a $CaF_2$ cell with a 50 μm spacer. Suspensions in buffered $^2H_2O$ of BSA

adsorbed on talc, or on montmorillonite, were inserted between two $CaF_2$ plates with a 25

μm spacer allowing an easy cleaning. Spectra at several $p^2H$ were recorded between 1350

and 1800 cm$^{-1}$ and from 6 min (minimum time for sampling) to 6 hours. Spectra of BSA in

solution, or adsorbed on the clay surfaces were obtained from the difference spectra (BSA +

buffer) - (buffer) and (BSA + clay + buffer) - (clay + buffer), respectively (Fig. 1). All spectra

are normalized on the maximum of the Amide I peak (15, 21-24). Important spectral changes

were detected between 6 min and 2 h, but not after 2 hours. The present analysis refers to

spectra recorded at 10 min and 2 h (Fig. 1).

Curve fittings were performed in the 1500-1750 cm$^{-1}$ region on the difference spectra

slightly smoothed to cancel the absorption of residual vaporized water (3 runs of an iterative

procedure on three points). Second derivative or curvature analyses (15) gave 16 overlapping

peaks at similar frequencies for any spectrum. Identical empirical half bandwidth at half

height (12 cm$^{-1}$) and profile (0.25 Gaussian /0.75 Lorentzian) were introduced to adjust all

components to get the best-averaged fit for all spectra. These parameters are fixed. The least-

square iterative curve-fitting program (Levenberg-Marquardt) only adjusts for each spectrum

the intensity parameter of each component (Fig. 2). These values are all expressed as

percentages of the overall Amide I absorption (15, 21-24). All components are assigned to

specific Amide and side-chain vibrations (21-24).

Components in the 1700-1750 cm$^{-1}$ range are related to the $\nu CO_{COOH}$ stretching

vibration for carboxylic Asp and Glu side-chains, the bands in the 1565-1585 cm$^{-1}$ range

assigned to the $\nu_a COO^-$ modes for corresponding deprotonated residues (Fig. 2). The

percentages in COO$^-$ species, over all Asp and Glu side chains are not evaluated from their

intensities in this complex spectral range. COO$^-$ fractions (%) are deduced from measurements

of the area of the $\nu CO_{COOH}$ absorption for the remaining COOH species (with respect to the

overall Amide I intensity at a given p$^2$H). These relative areas are expressed with respect to

the corresponding relative areas (%) obtained at low p$^2$H when Asp and Glu side-chains are

all fully protonated (100 % COOH). The COO$^-$ (%) content was obtained by difference. With

careful control of time, p$^2$H, temperature and spectrometer drying, there was less than 10 %

COO$^-$ variation for replicate samples.

Two components in the 1530-1550 cm$^{-1}$ are attributed to the Amide II peptide modes

involving NH motion (Fig. 2). The amount of remaining CONH peptide units at a given time

is expressed in % of the overall peptide units in BSA (15, 21-24). The sum of the areas of the

residual Amide II components is first referred to the overall Amide I band. The final value (%

peptide NH) accounts for the fact that for fully protonated BSA in solid state and dispersed in

a fluorolub mull, the Amide II/Amide I ratio is 0.5. There was less than 4 % peptide NH

variation between similar samples. As BSA contains 582 amino acids, a decrease in % NH by

~ 5 % indicates that ~ 30 peptide units are involved in NH/N$^2$H exchange. The level of

exchange at a given time depends on the rate at which water molecules gain access to internal

peptide groups in the protein core (15, 21-24, 29).

In the 1615-1690 cm$^{-1}$ range, seven peaks (Fig. 2) are assigned to peptide $\nu$CO vibrations involved in the Amide I/I' modes (CONH/CON$^2$H) (Table 1). The assignments are deduced from the literature (30-33) and from our own and other experiments on model amides (34, 35), polypeptides (36, 37) and proteins (15, 21-24). The level of the peptide NH/N$^2$H exchange being considerable in all the cases studied, it has not been necessary to introduce different frequencies for Amide I (CONH), and Amide I' (CON$^2$H) components (15, 21-24, 38). The list of Amide I components identified is given in Table 1.

*Peptide carbonyls, H-bonded in BSA secondary structures*

Internal and packed hydrophobic helical domains give rise to $\nu$CO frequencies slightly higher than peripheral and solvated helical domains (21-23, 39-44). Hence, the Amide I contribution for $\alpha$-helix in BSA involves two sub-components at 1660 and 1651 cm$^{-1}$, respectively. In solution, the overall helical domains involve about 60 % of the backbone. Other peptide CO groups are H-bonded in bent extended polypeptide strands. They absorb at *ca* 1630 cm$^{-1}$ and account for about 20 % of the backbone (Table 2) (21, 22).

*Peptide carbonyls, "free" in extended random internal structures*

Two distinct frequencies are attributed to "free" carbonyls in extended random internal structures. The 1681-cm$^{-1}$ component corresponds to carbonyls, which are free in hydrophobic, random, or bent domains. The 1670-cm$^{-1}$ component is also assigned to free carbonyls, but in more polar internal domains (34-37).

*Peptide carbonyls, involved in intermolecular H-bonds*

The 1640-cm$^{-1}$ component is ascribed to peptide carbonyls that are H-bonded to $^2$H$_2$O in random or bent domains, when exposed to the buffer. In this study, as in others (15, 21-24, 45), such absorption increases concomitantly with the rate of NH/N$^2$H exchange. The component at 1618 cm$^{-1}$ is associated to peptide units involved in protein self-association (15, 21-24, 46-48).

The area of each Amide I component is expressed as a percentage of the sum of the areas of all Amide I components. Intensities (% peptide CO) are used to deduce the proportion of peptide units involved in the various solvated structural domains of the BSA polypeptide backbone (Table 2). Variations were less than 1 % for replicate samples. For BSA, a variation of 1 % corresponds to structural and/or solvation changes involving about 6 peptide units.

## RESULTS

The %COO⁻ for Asp and Glu side chains, peptide $NH/N^2H$ exchanges and relative intensities for peptide CO components, are quantified for BSA in solution at 2 concentrations (Tables 2, 3) and for BSA adsorbed on montmorillonite or on talc (Tables 4, 5). The effects of $p^2H$ are first analyzed in each case from spectra recorded when structural and solvation equilibrium was reached at 2 h. Then, the time-dependent processes from 10 min to 2 h are compared for solutions and adsorbed states.

### Effect of concentration and $p^2H$ on structure of BSA in solution

For both solutions (30 and 4 g. $L^{-1}$), the $NH/N^2H$ exchange is greatly enhanced at $p^2H$ below the i.e.p. (Fig. 3A). This is correlated to increased direct hydration, which apparently results from significant $\alpha$-helix unfolding in relatively packed internal domains of the protein (Fig. 3B and D). These changes depend on the protonation of most of the Asp and Glu carboxylic side chains when the $p^2H$ becomes lower than their pK (Fig. 3C). Such protonation is assumed to cause a disruption of internal salt bridges between negatively and positively charged side chains of the protein. Such disruption and also internal repulsion forces between

uncompensated positive Arg, Lys and His ($R^+$) side chains are assumed to cooperatively induce the internal conformational transition involving about 8% of the backbone at low $p^2H$.

The largest amount of residual NH is observed at $p^2H$ 4.5 for the solution at 30 g. $L^{-1}$ but at $p^2H$ 5.2 for the solution at 4 g. $L^{-1}$ (Fig. 3A). Indeed, $p^2H$ dependent profiles for direct peptide hydration (Fig. 3B), for the amount of helix structure (Fig. 3D) and for peptide units involved in protein self-association (Fig. 3E) are all similarly shifted from concentrated to diluted solutions. The curves for %$COO^-$ also deviate in the same $p^2H$ range (Fig. 3C). At $p^2H$ higher than the pK of Asp and Glu side chains, many negatively charged side-chains interact with positively charged ones. Internal salt bridges favor helical structures and reduce protein self-association. Unexpectedly, in the 4-6 $p^2H$ range the amount of clustered protein (self-association) is larger for the diluted than for the concentrated solution (Fig. 3E). For the diluted solution statistically less numerous attractive and repulsive electrostatic forces between dissolved protein clusters could maintain aggregation until larger $p^2H$. Buried inside aggregates, even peripheral Asp and Glu side chains should have larger apparent pK values than when they are solvated by the buffer.

At $p^2H$ *ca* 6.2, self-association is totally concealed for both diluted and concentrated solutions. All the $p^2H$ dependent parameters are similar for both solutions. Compared to lower $p^2H$, a weak α-helix break is denoted. This small change in secondary structure could be generated by some His side chains becoming deprotonated, thus disrupting salt bridges between negative carboxylates and positive imidazole rings.


**Effects of adsorption on BSA structure and solvation**


*COO⁻/COOH equilibrium*

At $p^2H$ above 5, most of the carboxylic functions are deprotonated for both solutions and for BSA adsorbed on talc (Fig. 4). As displayed by the larger intensity of the $vCO_{COOH}$ absorption *ca* 1710 cm$^{-1}$, this is not the case for BSA adsorbed on montmorillonite.

For adsorption on montmorillonite carboxylic functions persist at least until $p^2H$ 6.5 (Fig. 4A). Various reasons may explain such a shift of the apparent pK (Asp, Glu). In the primary structure of BSA some Asp and Glu side-chains are adjacent to $R^+$ functions. Embedded among positively charged side chains interacting with the electronegative clay or embedded in self-associated domains, external Asp and Glu side chains are assumed to become indifferent to buffer. Moreover the electronegative charge of the clay surface could favor a protonation of the Asp and Glu carboxylates to decrease the coulombic repulsion between the protein and the surface, as observed by titration on other systems (49).

When interactions between BSA and clay are hydrophobic, as for talc, carboxylic side chains should not be perturbed. They remain influenced by the solvent as in the solution (Fig. 4B).

*CONH/CON$^2$H exchange*

Upon adsorption on montmorillonite, the amount of $p^2H$ dependent residual NH is inverted compared to solution (Fig. 5A). For acidic $p^2H$, the weaker exchange after adsorption suggests that the electronegative surface protects some domain of the protein. In contrast, in the i.e.p. range adsorption increases the NH/N$^2$H exchange, while at higher $p^2H$, the rate of water diffusion in no longer influenced by the adsorption.

For BSA adsorbed on talc the NH/N$^2$H exchange at the i.e.p. is weaker to that in the corresponding solution (Fig. 5B). The exchange is larger for the adsorbed state at increased $p^2H$. In addition, a break in the $p^2H$ profile appears around $p^2H$ 6 after 2 hours (Fig. 5B), as was already observed after 10 min (Table 5).

*Amide I components*

Diagrams in Figure 6 and 7 present the $p^2H$ dependence of the intensities of all the Amide I components for adsorbed BSA and the corresponding BSA solutions. Intensities reflect the amplitude of the conformational and solvation states of the polypeptide backbone after 2 hours.

Secondary structures

The amount of external and solvated $\alpha$-helices does not depend on $p^2H$ for either the adsorbed states or the solutions. However, adsorption on montmorillonite entails a loss in such helices, concerning on average ~ 10% of the backbone (Fig. 6A). Denaturation is weaker for adsorption on talc with only ~ 4% of unfolding in external/regular helices (Fig. 6C). The amount of bundled $\alpha$-helix domains and $p^2H$ dependent profiles for such structures differ considerably between solutions and adsorbed states (Fig. 6A and C). At the i.e.p., adsorption on montmorillonite strongly reduces the amount of bundled helices compared to the solution (~ 12%). Unfolding is much reduced at higher $p^2H$ when some His side chains deprotonate. In the similar $p^2H$ range, the amount of internal helical domains is also reduced for the adsorption on talc, but only in the 5.6-6.5 $p^2H$ range and less so than with montmorillonite. It should be noted that the $p^2H$ dependent profiles for bundled helices follow those observed for the decreases of the Amide II bands for both adsorbed and solution states. Unfolding of bundled/internal helical domains increases water diffusion inside the core of the protein (Fig. 5). At $p^2H < 7$, $\alpha$-helix unfolding is concomitant with slight enlargement of bent domains for both adsorbed states compared to solutions (Fig. 6B, D). In contrast, a peculiar decrease of such structure is noted with talc at $p^2H$ 7.3.

Random and self-associated domains

In solution, the amounts of free polar and hydrated peptide CO and of peptide CO in protein aggregation are the lowest in the 4.5-6.5 $p^2H$ range (Fig. 7), while the extension of internal α-helix domains is at a maximum (Fig. 6). This is not the case for either adsorbed state. Between $p^2H$ 4.8 and 6.7, helical unfolding on adsorption increases the amounts of self-association, free polar CO and hydrated peptide CO. Among the peptide units that are unfolded, those embedded in hydrophobic regions are probably responsible for the increase in protein self-association, the others in polar environments should become hydrated. On average, adsorption on montmorillonite entails a larger degree of protein self-association than on talc (Fig. 7A and C). The level of protein self-association on montmorillonite is even more important at low $p^2H$. In addition, throughout the $p^2H$ range 2.9-6.7, adsorption enhances the amount of free peptide CO in hydrophobic environments. Adsorption on talc rather limits the extension of such domains until $p^2H$ 6.5. The orientation of hydrophobic side chains towards the hydrophobic surface may have induced local disruptions in internal compact regions.

*Time-dependent processes*

-in solution

BSA molecules are self-associated after 2 h for BSA 30 g. $L^{-1}$ and 4 g. $L^{-1}$, until $p^2H$ 4.2 and 5.3, respectively (Fig. 3E). In these conditions the time-resolved study from 10 min to 2 hours shows specific slow structural transitions. A progressive unfolding of internal helical domains increases the amount of free peptide CO inside the protein and the direct backbone hydration (Tables 2, 3). At higher $p^2H$ when after 10 min, BSA is no longer self-associated and carboxylic functions all rapidly deprotonated, the time dependent structural and solvation changes are much weaker.

-on adsorption

For BSA adsorbed on montmorillonite, slow processes are also only observed at low $p^2H$. In this $p^2H$ range the discrepancies between solution and adsorbed states increase from 10 min to 2 h (Tables 2, 4). After 10 min, the primary unfolding concerns external α-helical regions (~ 7% of the protein) when several uncompensated $R^+$ external side chains are rapidly neutralized by the electronegative montmorillonite. At $p^2H$ 2.9 about 4% of the backbone located in external helical domains and 6% in internal domains unfold more slowly (Table 4). However in contrast with the solution, on adsorption the slow process does not entail backbone hydration, but strongly favor BSA self-association. In solution uncompensated positively charged side chains were assumed to create repulsive forces generating protein unfolding. After adsorption, because a proportion of the positively charged groups is held on the electronegative surface and because the carboxylic groups are protonated, repulsive forces between adsorbed adjacent BSA molecules are much less than for either the protein in solution at the same $p^2H$ or that adsorbed at higher $p^2H$. Self-association is progressively favored.

In the $p^2H$ range studied, most of the structural transitions are already complete after 10 min (Table 5). Adsorption on talc is mainly a fast process.

## DISCUSSION

Measurements of the $COO^-/COOH$ ratio, peptide $NH/N^2H$ exchange and peptide CO intensities give interdependent conclusions leading to a coherent comparative description of BSA conformation in solution, adsorbed on montmorillonite, or on talc, at different $p^2H$ and times.

**Unfolding process for BSA adsorbed on montmorillonite**

Adsorption of BSA in the $p^2H$ range 4.3-5.6 induces a large structural transition compared to solution. External as well as internal $\alpha$-helix domains are unfolded. All processes involve about 20% of the backbone. Differences are already established after 10 min. The movement of $R^+$ side chains towards the clay-surface, and the corresponding unpairing of some carboxylate side chains, is the major process which causes structural change. Interactions of external $R^+$ side chains with the clay-surface would induce helical unfolding in external domains ($\sim$ 9% of CO peptide units). A proportion of these peptide units becomes hydrated. Others situated between hydrophobic segments favor protein self-association to some extent. Because the structural transition also involves internal domains ($\sim$ 10%) and increases water diffusion into the protein core, we conclude that some inner $R^+$ side chains are transferred towards the surface of the clay. The adjacent unpaired carboxylate functions are responsible for the increased inner hydration. Some of the internal denatured segments remain without interaction with water, as shown by the increase of "free" peptide units in polar and hydrophobic domains.

At $p^2H$ 6.7, in spite of the slightly electronegative character of BSA, adsorption occurs, but helix unfolding only concerns peripheral domains ($\sim$ 10% CO units). Only due to the hindrance of the clay, in contrast to lower $p^2H$, internal domains of adsorbed BSA become less accessible to water than in solution at same $p^2H$.

For $p^2H$ 2.9, the behavior of adsorbed BSA does not follow the same trend as in solution. For adsorption, after 10 min, a fast unfolding only concerns external $\alpha$-helical regions when several unbalanced $R^+$ external side chains are rapidly neutralized by the electronegative montmorillonite. A slow structural transition involves both external and internal helical domains. At equilibrium the level of hydration becomes similar for solution

14

and adsorbed state but, this level is reached through different kinetics. For the adsorbed state

the hydration of polar unfolded external domains was rapidly established within 10 min. The

helical domains that are later unfolded probably contain hydrophobic segments explaining the

protein self-association. This self-association is more favored at $p^2H$ 2.9 than at $p^2H$ 4.5

because protonated Asp and Glu side chains do not generate electronegative repulsive forces

between adsorbed adjacent protein molecules.

This FTIR study gives information complementary to the NMR study performed on

the same system (17, 50). The NMR approach was devised to measure the area of the interface

between a BSA macromolecule and montmorillonite by following the release of a

paramagnetic cation from the clay surface on protein adsorption. The paramagnetic cation

released in the solution was detected by its interaction with orthophosphate by ^{31}P-NMR

spectroscopy. It was calculated from these NMR data that the specific interfacial area of BSA

on montmorillonite at the i.e.p. should be around 60 $nm^2$. Since this value was compared to

the pre-1992 model of serum albumin (51), which assumed an ellipsoid-shaped protein

("cigar-shaped") of 14 nm x 4 nm, it was concluded that at the i.e.p. there was no extensive

unfolding of the BSA on the clay surface, since the observed and theoretical interfacial areas

were very similar. This conclusion was thought to be erroneous when the X-ray structure of

HSA was finally elucidated in 1992 (26). The shape of HSA is in fact an equilateral triangle

with sides of 8 nm and a depth of 3 nm ("heart-shaped"). Thus the interfacial area of contact

of a serum albumin with native structure adsorbed "side-on" on a surface should be 28 $nm^2$,

which is approximately half the value observed by NMR spectroscopy. Thus, at this pH, the

protein must be unfolded. The FTIR data presented here, showing an extensive modification

of the secondary structure of the protein, support this hypothesis of an unfolding at the i.e.p.

This conclusion is in good agreement with the low structural stability of the serum albumins

(16, 18).

Serum albumin behavior near electrostatic surfaces depends also strongly on whether the surface is electronegative or electropositive. For example, previous results on the very similar human serum albumin, HSA, adsorbed on a silica support coated with positively charged polyvinylimidazole, (PVI) showed only very weak structural perturbations for albumin, although it can be strongly retained on the polymer which coats about 50% of the solid surface (24). Interaction of external carboxylate side chains with the electropositive surface apparently affects HSA secondary structure much less (- 4% in bundled helices), than does the adsorption of BSA onto montmorillonite, via $Lys^+$ and $Arg^+$ side chains alone, or also via His side chains, when protonated. The contrast between the effects of these two electrically charged surfaces probably lies in the difference in their surface charge density and the chemical nature of the adsorbing surface. The differences could also be related to the length of the outwarding pointing alkyl chains in the two systems. In the case of adsorption on PVI-silicate, these are short Asp and Glu alkyl chains, whereas for montmorillonite they are the longer Arg and Lys with functional groups on the positions $\gamma$ or $\delta$ of the $\alpha$ carbon, respectively. The more flexible Arg and Lys side chains would have a greater chance to approach surfaces than Asp and Glu side chains. The denaturating effect of $His^+$ side chain adsorption of at $p^2H$ below the $pK_{His}$ is also a very specific characteristic of protein adsorption on electronegative supports.

**Unfolding process for BSA adsorbed on talc**

At $p^2H$ 4.8, in contrast to adsorption on montmorillonite and compared to the diluted solution, adsorption on talc only unfolds external helical domains. The helix-loss (~ 7% of the backbone) and the decrease in hydrophobic domains (2%) are balanced by increased polar

(2%), hydrated (2%) and self-associated (2%) domains. BSA is adsorbed on talc via peripheral

hydrophobic regions and maintains the same internal conformation as in solution.

Results for $p^2H$ 5.6, imply that adsorption on clay also involves one helical domain

that was packed in solution, specifically in this $p^2H$ range. This domain should be

amphiphatic. When its hydrophobic side chains are orientated towards the clay, the polar ones

may drift out from specific internal location for BSA in solution. Self-association confirms

that unfolded domains on adsorption contain hydrophobic segments. They also contain

hydrophilic side chains to explain the larger hydration confirmed by greater water diffusion.

The unfolding of BSA due to its adsorption on talc (7-9%) is lower than the

unfolding resulting from the adsorption of HSA on a reversed chromatographic phase grafted

with hexyl chains (12%) (21). The embedding of HSA hydrophobic side chains among the

flexible grafted hexyl chains could perturb more albumin secondary structures than the

approach of similar side chains of BSA towards the rigid oxygen network at the talc surface.

**Role of Asp, Glu and His side-chains in BSA structure**

In solution, BSA structure depends on protonation states of Asp and Glu carboxylic

functions and His side-chains in the pH range studied. The amount of internal helix is favored

when carboxylic side-chains are deprotonated, while His side chains still protonated. Salt

bridges between $COO^-$ and $His^+$ are assumed to cause folding in internal BSA regions. Such a

specific increase in helicity in the range $4 > p^2H > 5.6$ is not observed for either adsorbed

states.

At low $p^2H$, without repulsive forces due to carboxylates, self-associated BSA

molecules can spread over montmorillonite-surface. For $p^2H$ between the pK values of the

constituent monomers, pK (Asp, Glu) $< p^2H <$ pK (His) some carboxylic side chains

embedded at the BSA/clay interface remain protonated. On the other hand, some $His^+$ side-

chains should be oriented towards the electronegative surface. Both effects may cooperatively restrict the formation of helix-promoting internal salt bridges. For $p^2H$ 6.7, after His deprotonation, these side chains are no longer attracted to the electronegative clay whereas in solution the helix-promoting salt bridges are disrupted, thus the structural changes from solution to adsorption become less marked.

The protonation of Asp and Glu carboxylates of BSA adsorbed on montmorillonite occurs at pH largely above their pK for the protein in solution. This could be related to the role, in the reduction of coulombic repulsion, of the transfer of ions from the solution to the adsorbed layer of protein (16, 18, 49, 52, 53). This transfer of ions decreases the magnitude of the repulsion between like-charged parts of the protein and the surface in an interfacial region of low dielectric permittivity. Any cation from the solution, including protons, can be transferred. Our results point to the importance of proton transfer to the protein layer in this process. This phenomenon could explain the pH increase observed when a solution of protein and a clay suspension, both with the same original pH and unbuffered, are mixed (5).

For BSA adsorbed on talc the carboxylic functions are deprotonated at similar $p^2H$ as in solution. The lack of folding in the intermediate range of $p^2H$, pK (Asp, Glu) < $p^2H$ < pK (His), compared to the solution implies that, as for adsorption on montmorillonite, structurally determinant $His^+$ and $COO^-$ functions are displaced during the unfolding of the amphiphatic BSA domain that adsorbs on the talc. However, part of the internal folding is recovered in the $p^2H$ range 6.2-6.5, just when some $His^+$ becomes neutral. This emphasizes that at $p^2H$ 5.6, adsorption via hydrophobic residues, thereby unpairing $His^+$ side chains, impedes the distal salt bridge that promoted helix formation in solution. Indeed, the level of internal helices is once more very similar to that in solution at $p^2H$ 7.3 when most of $His^+$ side chains are deprotonated. Only $p^2H$ independent unfolding in external domains is maintained. Similarly, water diffusion inside the core of BSA is not greater than in solution.

CONCLUSION

This study, exclusively deduced from an FTIR analysis, provides direct and original information at a molecular level on structural and solvation features of adsorbed albumin. The results are in agreement with the NMR analysis of the pH-dependent variation of BSA-montmorillonite interfacial area (17), whose comparison with the dimensions of the X-ray deduced structure of the homologous HSA (26) indicates a low structural stability since an unfolding on the surface is observed even at the i.e.p.. The FTIR analysis of interaction with montmorillonite of BSA (this work) and $\alpha$-chymotrypsin (15) shows an extensive modification of the secondary structure of the former on adsorption compared with a minimal modification of the latter. Thus, according to their stability at solid-liquid interfaces, the BSA is a "soft" protein and the $\alpha$-chymotrypsin is a "hard" protein.

For BSA, the dependence on $p^2H$ of the proportion of helices is very different in solution and in adsorbed states. After adsorption on montmorillonite, the largely $p^2H$ independent external helix unfolding is related to new orientations for the $Lys^+$ and $Arg^+$ side chains forced close to the negative clay surface. In contrast, unfolding in internal and packed helices is largely $p^2H$ dependent. This change is connected to the disruption of some $(Asp^-/Glu^-)\text{-}His^+$ salt bridges that enhance helix formation in solution. Indeed, adsorption involves protonated $His^+$ as proved by the recovery of helices when all His side chains become deprotonated. At low $p^2H$, the protein molecules adsorbed on montmorillonite spread over the entire mineral surface, which is in agreement with the instability of BSA structure in solution. These molecules are largely self-associated. At higher $p^2H$, uncompensated Asp or Glu carboxylates limit the self-association of the adsorbed units.

Adsorption of BSA on the neutral talc is, on average, less destructive than adsorption on the negative montmorillonite, but surprisingly structural effects are also $p^2H$ dependent. At $p^2H$ 4.8, only external helical domains are unfolded after adsorption on talc. Bundled internal helical domains are not at their optimum level either in solution or in the adsorbed state because some internal carboxylic functions are not yet deprotonated. At $p^2H$ 5.6 the salt bridges that induce local helix folding in solution cannot be established when BSA is adsorbed on talc. The adsorption of external amphiphatic domains impedes the salt bridge formation. Internal impaired charges cause specific hydration.

We emphasize on the importance of electrostatic forces in protein adsorption processes whether adsorptive minerals are negatively charged or neutral. In the first case, the charges on the side chains influence the adsorption as a function of $p^2H$. In the second case, hydrophobic interactions at the protein-clay interface may also distort bundled domains at various distances from the interface. Asp, Glu and His side chains play a major role in both ternary and secondary BSA structures. For $p^2H$ large enough to ensure complete Asp and Glu deprotonation, the major $p^2H$ and adsorption effects are already established after 10 min. For low $p^2H$, when Asp and Glu are protonated, slow conformational rearrangements depend on protein concentration and on the adsorptive surfaces leading to different structures with various protein self-association over protein hydration ratio.

Finally this study shows that proton transfer from the solution to the adsorbed layer of BSA on montmorillonite occurs, as demonstrated by the higher protonation of Asp and Glu carboxylic groups for the adsorbed protein than in solution. This phenomenon reduces the unfavorable coulombic repulsion between like-charged parts of the BSA and the electronegative montmorillonite surface.

REFERENCES

1.  Horbett, T. A., and Brash, J. L., "Proteins at Interfaces II: Fundamentals and Applications", ACS Symposium Series **602**, American Chemical Society, Washington, 1995.

2.  Theng, B. K. G., *in* "Formation and Properties of Clay-Polymer Complexes" (B. K. G. Theng, Ed.), pp. 157. Elsevier, Amsterdam, 1979.

3.  Armstrong, D. E., and Chesters, G., *Soil Sci.* **98**, 39 (1964).

4.  Albert, J. T., and Harter, R. D., *Soil Sci.* **115**, 130 (1973).

5.  Fusi, P., Ristori, G. G., Calamai, L. and Stotzky, G. *Soil Biol. Biochem.* **21**, 911 (1989).

6.  Violante, A., De Cristofaro, A., Rao, M. A., and Gianfreda, L., *Clay Miner.* **30**, 325 (1995).

7.  McLaren, A. D., *J. Phys. Chem.* **58**, 129 (1954).

8.  Burns, R. G., *in* "Soil Enzymes" (R. G. Burns, Ed.), pp. 295. Academic Press, New York, 1978.

9.  Burns, R. G., *Soil Biol. Biochem.* **14**, 423 (1982).

10. Quiquampoix, H., *Biochimie* **69,** 753 (1987).

11. Quiquampoix, H., *Biochimie* **69,** 765 (1987).

12. Quiquampoix, H., Chassin, P., and Ratcliffe, R. G., *Prog. Colloid Polym. Sci.* **79,** 59 (1989).

13. Gianfreda, L., and Bollag, J. M., *Soil Sci. Soc. Am. J.* **58**, 1672 (1994).

14. Leprince, F., and Quiquampoix, H., *Eur. J. Soil Sci.* **47**, 511 (1996).

S. Servagent-Noinville, M. Revault, H. Quiquampoix and M.H. Baron,  Journal of Colloid and
Interface Science 221 (2000) 273-283.

DOI: 10.1006/jcis.1999.6576

15. Baron, M. H., Revault, M., Servagent-Noinville, S., Abadie, J., and Quiquampoix,
H., *J. Colloid Interface Sci*. (1999, in press).

16. Norde, W., *Adv. Colloid Interface Sci.* **25**, 267 (1986).

17. Quiquampoix, H., and Ratcliffe, R.G., *J. Colloid Interface Sci.* **148**, 343 (1992).

18. Haynes, C. A., and Norde, W., *Colloids Surf. B Biointerfaces* **2**, 517 (1994).

19. Staunton, S., and Quiquampoix, H., *J. Colloid Interface Sci.* **166**, 89 (1994).

20. Quiquampoix, H., Abadie, A., Baron, M. H., Leprince, F., Matumoto-Pintro, P. T.,
Ratcliffe, R. G., and Staunton, S., in "Proteins at Interfaces II: Fundamentals and
Applications", ACS Symposium Series **602**, p.321. American Chemical Society,
Washington, 1995.

21. Boulkanz, L., Balcar, and Baron, M. H., *Applied Spectrosc*. **49**, 1737 (1995).

22. De Collongue, B., Sebille, B. and Baron, M. H., *Biospectros*. **2**, 101 (1996).

23. Boulkanz, L., Vidal-Madjar C., Balcar, N., and Baron, M. H., *J. Colloid Interface
Sci*. **188**, 58 (1997).

24. Pantazaki, A., Baron, M. H., Revault, M., and Vidal-Madjar C., *J. Colloid Interface
Sci*. **207**, 324 (1998).

25. Chassin, P., Jouany, C., and Quiquampoix, H., *Clay Miner.* **21,** 899 (1986).

26. He, X. M., and Carter, D. C., *Nature* **358**, 209 (1992).

27. Carter D. C., and Ho, J. X., *Adv. Protein Chem*. **45**, 153 (1994).

28. Glasoe, P. K., and Long, F. A., *J. Phys. Chem*. **64**, 188 (1960).

29. Gregory, R. B., and Rosenberg, A., *Methods Enzymol*. 131 448 (1986).

30. Arrondo, J. L. R., Muga, A., Castresana, J., and Goni, F. M., *Prog. Biophys. Molec. Biol*. **59**, 23 (1993).

31. Byler, D. M., and Susi, H., *J. Ind. Microbiol*. **3**, 73 (1988).

32. Byler, D. M., and Susi, H., *Biopolymers* **25**, 469 (1986).

33. Surewicz, W. K., and Mantsch, H. H., *Biochim. Biophys. Acta* **952**, 115 (1988).

34. Baron, M. H., de Loze, C., and Fillaux, F., *Biopolymers* **11**, 2063 (1972).

35. de Loze, C., Baron, M. H., and Fillaux, F., *J. Chimie Physique* **75**, 632 (1978).

36. Baron, M.H., de Lozé, C., Toniolo, C. and Fasman, G.D, *Biopolymers,* **17**, 2225 (1978).

37. Hollòsi, M., Majer, Z. S., Rònai, A. Z., Magyar, A., Medzihradszky, K., Holly, S., Perczel, A., and Fasman, G. D., *Biopolymers* **34,** 177 (1994).

38. Caughley, B. W., Dong, A., Bhat, K. S., Ernst, D. S. F., and Caughey, W. S., *Biochemistry* **30**, 7672 (1991)

39. Goormaghtigh, E., Vigneron, L., Knibiehler, M., Lazdunski C., and Ruysschaert, J. M., *Eur. J. Biochem*. **202**, 1299 (1991).

40. Rothschild, K.J., and Clark, N.E., *Biophys. J.* **25**, 473 (1979).

41. K. Matsuzaki, K, Shioyama, T., Okamura, E., Umenura, J, Takenaka, T., Takaishi, Y., Fujita, T., and Miyajima, K., *Biochim. Biophys. Acta* **1070**, 419 (1991).

42. Zhou, N. E., Zhu, B.,Y., Sykes, B., D. and Hodges, R., S., *J. Am. Chem. Soc.* **114**, 4320 (1992).

43. Pezolet, M., Bonenfant, S., Dousseau, F., and Popineau, Y., *FEBS Letter* **299**, 247 (1992).

44. Dousseau, F., and Pezolet, M., *Biochemistry* **29**, 8771 (1990).

45. Wantyghem, J., Baron, M.H., Picquart, M., and Lavialle, F., *Biochemistry* **29**, 6600 (1990).

46. Arrondo, J. L., Young, N., Martini, N., Mantsch H.H., and Henry, H*., Biochim. Biophys. Acta* **952**, 261 (1988).

47. Baron, M.H., and Quiquampoix, H., in V[th] International Conference on the Spectroscopy of Biological Molecules, (T. Theophanides, J Anastassopoulou, and N Fotopoulos, Eds.) p. 109, Kluwer Acad. Publi., Dordrecht, 1993.

48. Jackson, M., and Mantsch, H. H., *Biochim. Biophys. Acta* **1118**, 139 (1992).

49. Norde, W., and Lyklema, J., *J. Colloid Interface Sci.* **66**, 266 (1978).

50. Quiquampoix, H., Staunton, S., Baron, M. H., and Ratcliffe, R. G., *Colloids Surf. A Physicochem. Eng. Aspects* **75**, 85 (1993).

51. Peters, T., Jr, *Adv. Protein Chem.* **37**, 161 (1985).

52. Van Dulm, P., Norde, W., and Lyklema, J., *J. Colloid Interface Sci.* **82**, 77 (1981).

53. Norde, W., *Colloids Surf.* **10**, 21 (1984).

# Tables

**Table 1. Frequencies and assignments of the Amide I components for BSA in $^2H_2O$ solution.**

| Frequency ($cm^{-1}$) | Assignments to $v(CO)$ peptide groups |
|---|---|
| 1681 | 'Free' CO in hydrophobic environment |
| 1670 | 'Free' CO in polar environment |
| 1660 | H-bonded CO in bundled internal $\alpha$-helices |
| 1651 | H-bonded CO in external $\alpha$-helices |
| 1640 | Hydrated CO |
| 1630 | H-bonded CO in bent or extended stands |
| 1618 | Intermolecular H-bonded CO in protein self-association |

**Table 2.** Percentages (%) for peptide CO (Amide I components) and residual peptide NH, for BSA in buffered solution at 30 g. $L^{-1}$ at t = 10 min. Changes from 10 min to 2 h are expressed as: $\Delta x$ = % (t = 2 h) - % (t = 10 min).

| $p^2H$ | 3.1 | 4.2 | 4.5 | 5.7 | 6.4 |
|---|---|---|---|---|---|
| Peptide carbonyls (%) | 10' / $\Delta x$ | 10' / $\Delta x$ | 10' / $\Delta x$ | 10' / $\Delta x$ | 10' / $\Delta x$ |
| Hydrophobic | 7/-2 | 7/-3 | 5/-1 | 4/-1 | 3/0 |
| Polar | 7/+3 | 5/+3 | 6/0 | 8/0 | 8/0 |
| Bundled helix | 19/-8 | 24/-8 | 26/-2 | 23/-1 | 21/-2 |
| External helix | 34/0 | 34/+4 | 36/+1 | 37/0 | 39/-2 |
| Hydration | 16/+4 | 13/+1 | 11/+2 | 11/+1 | 11/+1 |
| Bents | 14/+2 | 16/+2 | 16/0 | 17/+1 | 18/+2 |
| Self-association | 3/+1 | 1/+1 | 0/0 | 0/0 | 0/+1 |
| Peptide NH (%) | 30/-29 | 44/-22 | 48/-14 | 45/-13 | 41/-6 |

**Table 3.** Percentages (%) for peptide CO (Amide I components) and residual peptide NH, for BSA in buffered solution at 4 g. $L^{-1}$ at t = 10 min. Changes from 10 min to 2 h are expressed as: $\Delta$x = % (t = 2 h) - % (t = 10 min).

| $p^2H$ | 2.7 | 4.3 | 4.8 | 5.3 | 6.3 | 6.6 | 7.4 |
|---|---|---|---|---|---|---|---|
| Peptide carbonyls (%) | 10' / $\Delta x$ | 10 ' / $\Delta x$ | 10' / $\Delta x$ | 10' / $\Delta x$ | 10' / $\Delta x$ | 10' / $\Delta x$ | 10' / $\Delta x$ |
| Hydrophobic | 7/-2 | 6/-2 | 8/-4 | 8/-4 | 5/-2 | 3/0 | 1/0 |
| Polar | 7/+3 | 7/+3 | 6/+4 | 6/+2 | 7/+1 | 8/0 | 10/0 |
| Bundled helix | 18/-7 | 17/-6 | 20/-9 | 23/-4 | 21/-2 | 19/-2 | 15/-2 |
| External helix | 34/-1 | 35/0 | 33/+2 | 32/+5 | 35/+1 | 37/-1 | 39/0 |
| Hydration | 18/+3 | 16/+4 | 13/+5 | 11/+2 | 11/+2 | 11/+2 | 12/+2 |
| Bents | 13/+3 | 15/+1 | 17/+1 | 18/0 | 20/0 | 20/0 | 21/+1 |
| Self-association | 3/+1 | 4/+1 | 3/0 | 2/0 | 1/0 | 1/+1 | 2/0 |
| Peptide NH (%) | 34/-26 | 28/-23 | 40/-30 | **54/-23** | **45/-13** | **39/-10** | **31/-12** |

**Table 4.** Percentages (%) for peptide CO (Amide I components) and residual peptide NH, for BSA at 30 g. $L^{-1}$ adsorbed on montmorillonite at t = 10 min. Changes from 10 min to 2 h are expressed as: $\Delta$x = % (t = 2 h) - % (t = 10 min).

| $p^2H$ | 2.9 | 4.3 | 5.6 | 6.7 |
|---|---|---|---|---|
| Peptide carbonyls (%) | 10' / $\Delta x$ | 10' / $\Delta x$ | 10' / $\Delta x$ | 10' / $\Delta x$ |
| Hydrophobic | 9/0 | 7/-1 | 6/0 | 6/0 |
| Polar | 8/0 | 10/0 | 11/0 | 9/0 |
| Bundled helix | 20/-6 | 16/-3 | 15/-3 | 18/-2 |
| External helix | 27/-4 | 27/-1 | 27/-2 | 28/-2 |
| Hydration | 17/0 | 19/0 | 18/+1 | 16/+1 |
| Bents | 14/+4 | 16/+4 | 18/+3 | 19/+2 |
| Self-association | 5/+6 | 5/+1 | 5/+1 | 4/+1 |
| Peptide NH (%) | 36/-10 | 29/-9 | 31/-9 | 38/0 |

**Table 5.** Percentages (%) for peptide CO (Amide I components) and residual peptide NH, for BSA at 4 g. L$^{-1}$ adsorbed on talc at t = 10 min. Changes from 10 min to 2 h are expressed as: $\Delta x$ = % (t = 2 h) - % (t = 10 min).

| p$^2$H | 4.8 | 5.6 | 6.2 | 6.5 | 7.3 |
|---|---|---|---|---|---|
| Peptide carbonyls (%) | 10' / $\Delta x$ | 10' / $\Delta x$ | 10' / $\Delta x$ | 10' / $\Delta x$ | 10' / $\Delta x$ |
| Hydrophobic | 3/*0* | 4/*-2* | 4/*-2* | 4/*-2* | 4/*-1* |
| Polar | 10/*+2* | 10/*+2* | 9/*+1* | 9/*+2* | 9/*0* |
| Bundled helix | 15/*-3* | 15/*-3* | 16/*-2* | 16/*-3* | 14/*-1* |
| External helix | 31/*-3* | 32/*0* | 31/*-1.5* | 29/*+1* | 32/*0* |
| Hydration | 18/*+2* | 17/*+2* | 16/*+3* | 17/*+2* | 16/*+2* |
| Bents | 20/*0* | 19/*+2* | 21/*0* | 21/*0* | 20/*+1* |
| Self-association | 3/*+2* | 3/*0* | 3/*+1* | 4/*0* | 5/*0* |
| Peptide NH (%) | 42/*-15* | 34/*-12* | 38/*-12* | 30/*-11* | 23/*-8* |

27

## Figures and Figure captions
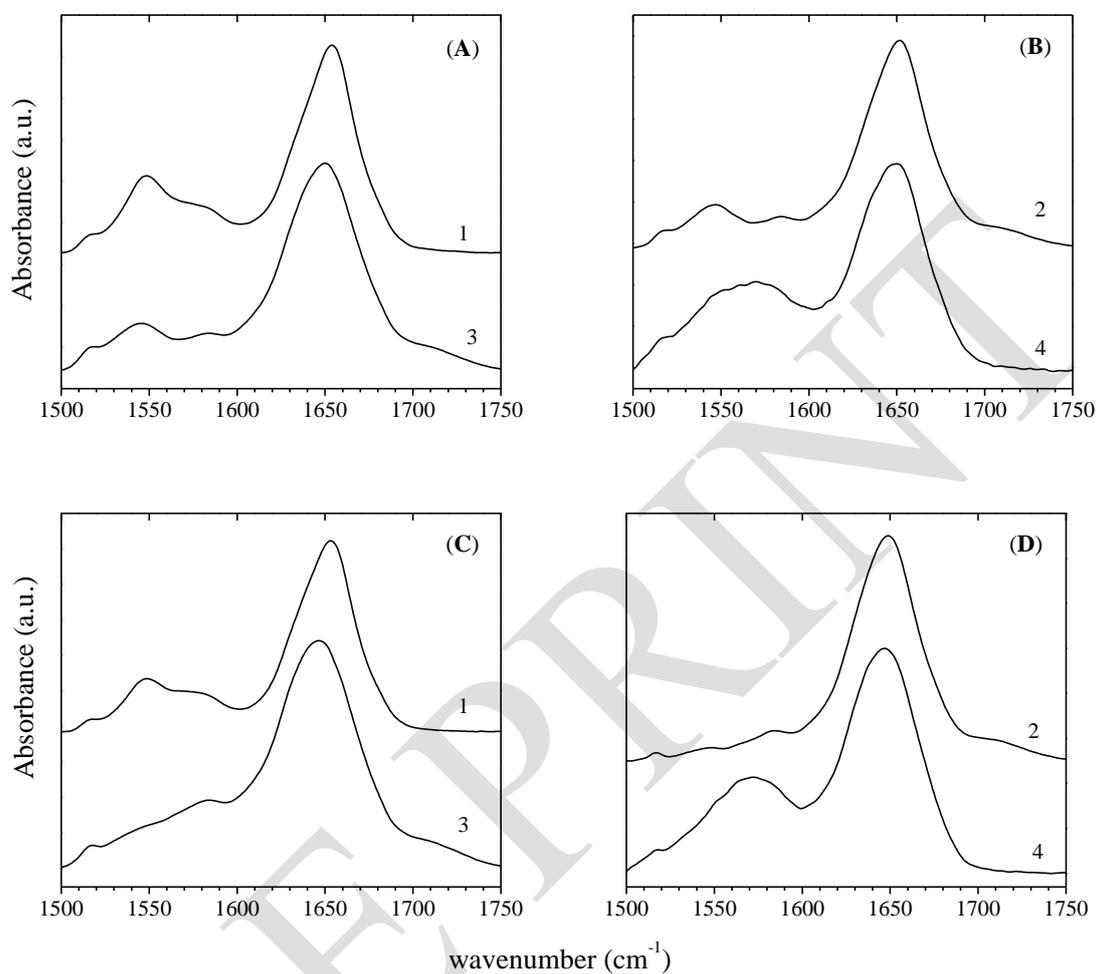


**Figure 1.** BSA infrared spectra at t = 10 min (A) and (B), and at t = 2 h (C) and (D). BSA in

solution at 30 g. $L^{-1}$ and $p^2H$ 4.5 (1); at 4 g. $L^{-1}$ and $p^2H$ 4.3 (2); BSA (30 g. $L^{-1}$) adsorbed on

montmorillonite at $p^2H$ 4.3 (3); BSA (4 g. $L^{-1}$) adsorbed on talc at $p^2H$ 4.8 (4).
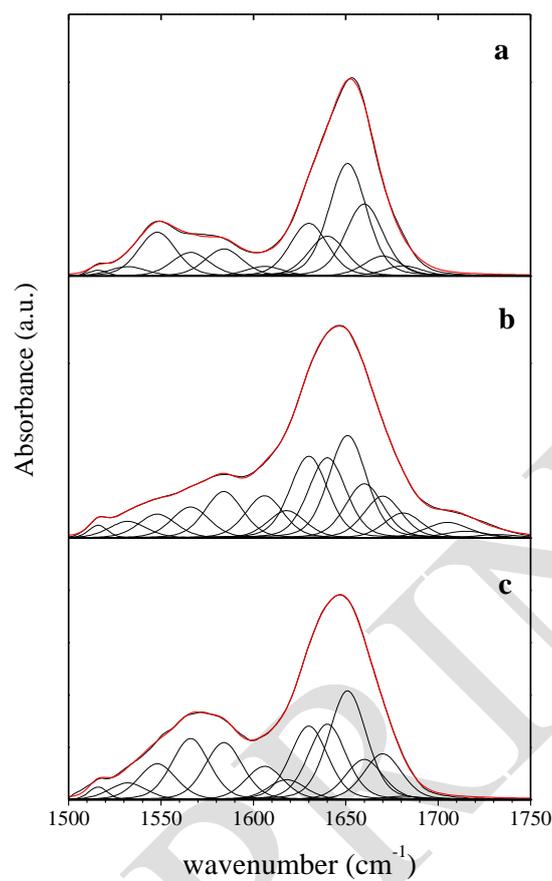
**Figure 2.** Decomposition of the infrared spectra of BSA at t = 2 h. BSA in solution, 30 g. L$^{-1}$ and p$^2$H 4.5 (a); BSA (30 g. L$^{-1}$) adsorbed on montmorillonite, p$^2$H 4.3 (b); BSA (4 g. L$^{-1}$) adsorbed on talc, p$^2$H 4.8 (c).
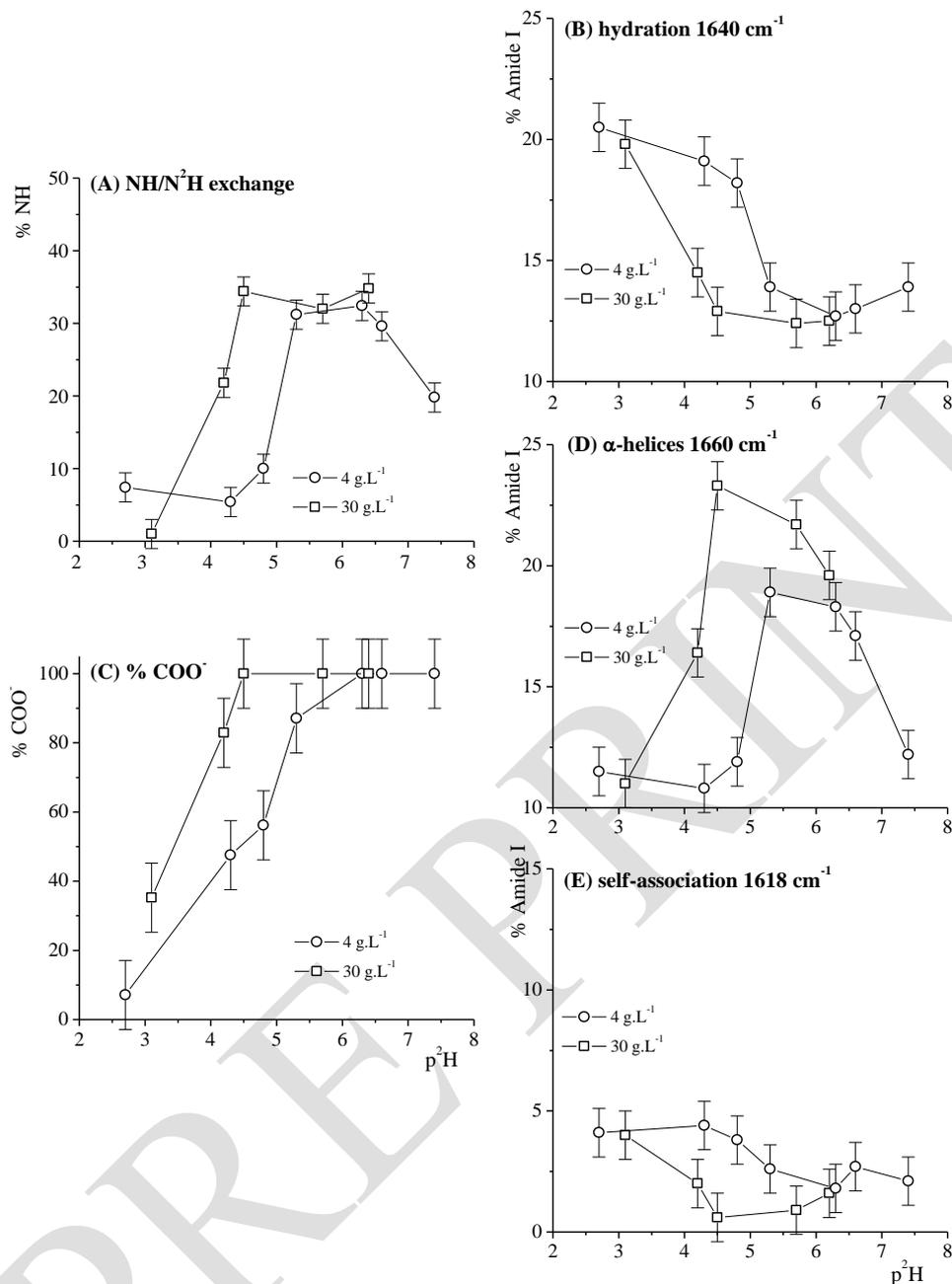
**Figure 3.** For various $p^2H$ at t = 2 h, effects of BSA concentration on : the amount of residual peptide NH (% of the overall peptide units) (A); the amount of hydrated peptide carbonyls (% of Amide I component at 1640 cm$^{-1}$) (B); the amount of Asp and Glu COO$^-$ (% of the overall Asp and glu side chains) (C); the amount of bundled α-helice (% of Amide I component at 1660 cm$^{-1}$) (D); the amount of peptide units involved in BSA self-association (% of Amide I component at 1618 cm$^{-1}$) (E).
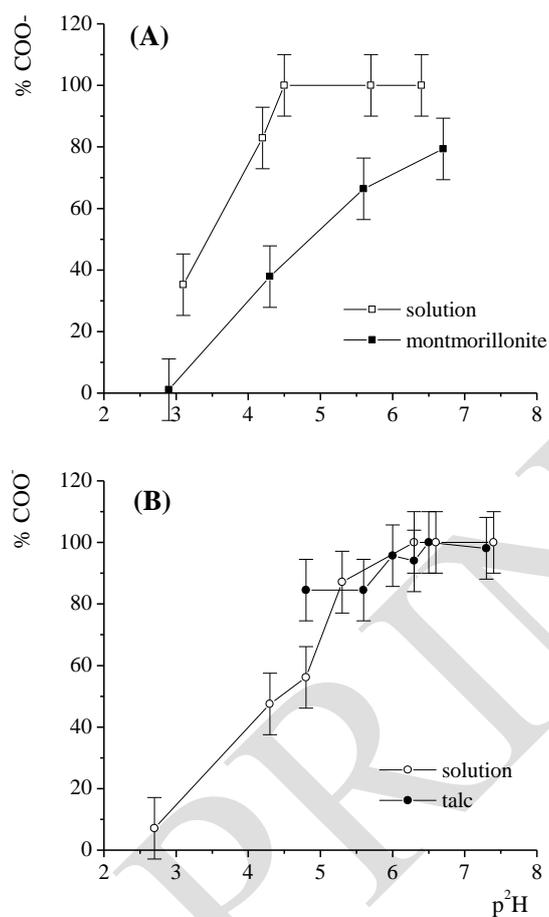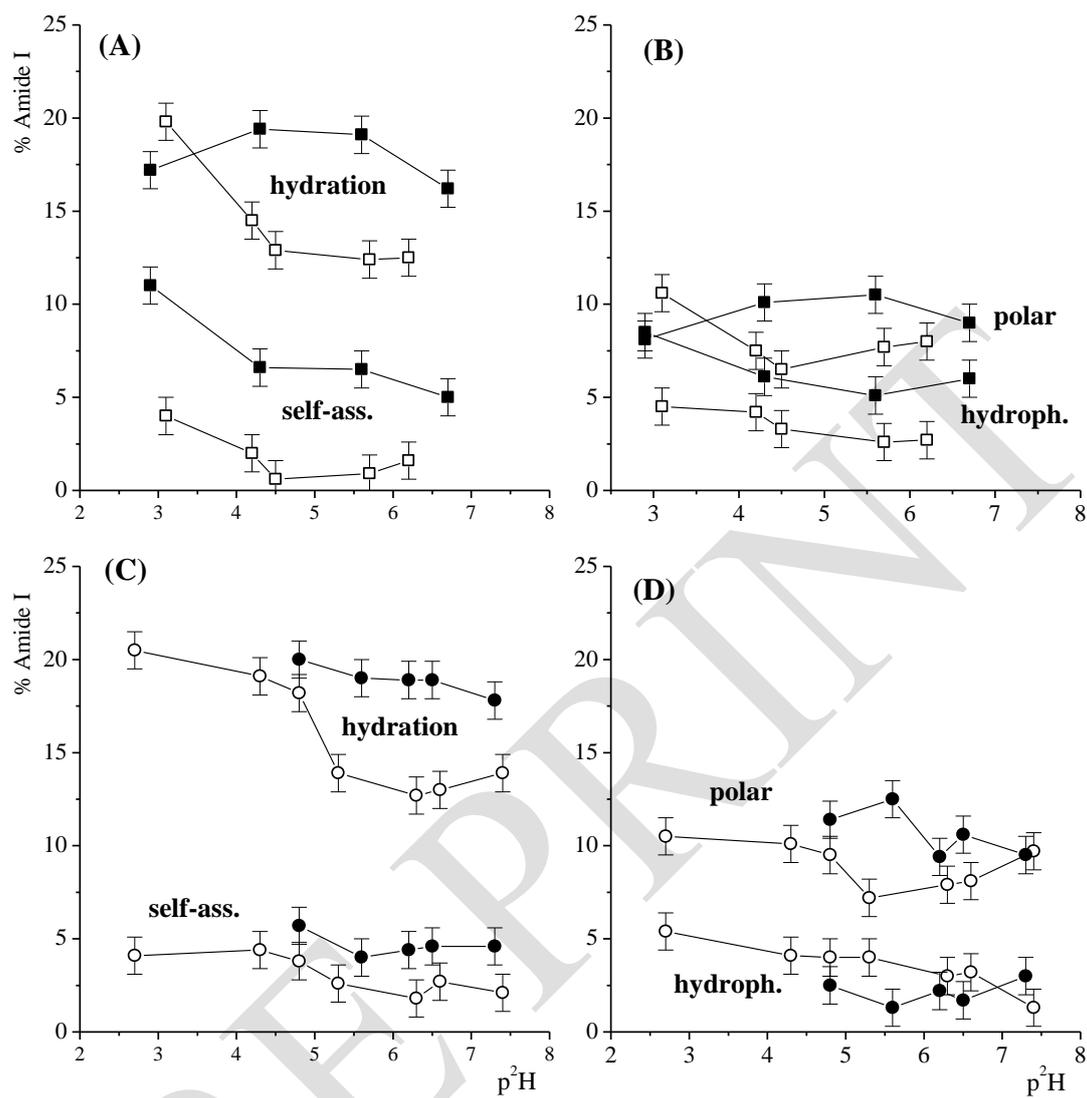
**Figure 4.** Comparison of %COO$^-$ for various p$^2$H at t = 2 h. BSA in solution at 30 g. L$^{-1}$ or adsorbed on montmorillonite (A); BSA in solution at 4 g. L$^{-1}$ or adsorbed on talc (B)
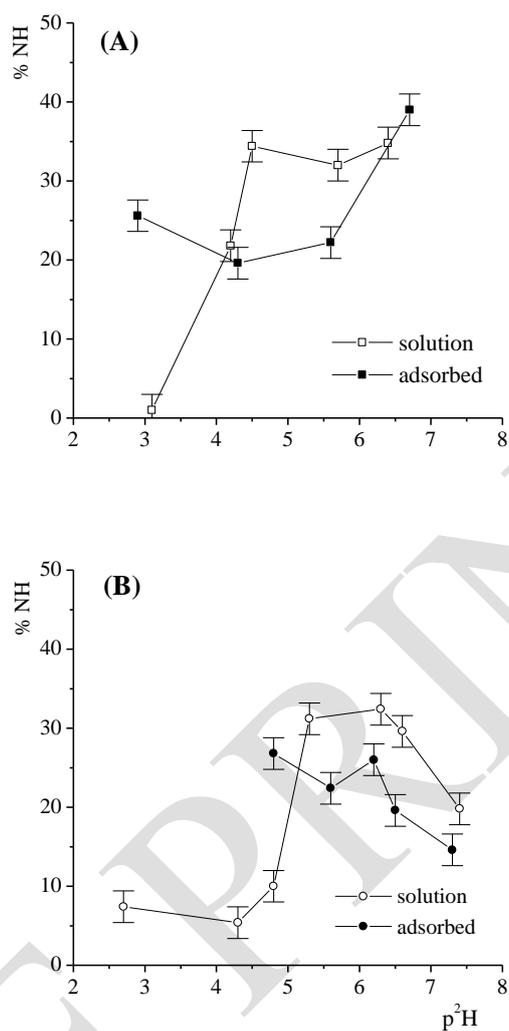
**Figure 5.** Comparison of %NH/N$^2$H ratio for various p$^2$H at t = 2 h. BSA in solution at 30 g.

L$^{-1}$ or adsorbed on montmorillonite (A); BSA in solution at 4 g. L$^{-1}$ or adsorbed on talc (B)
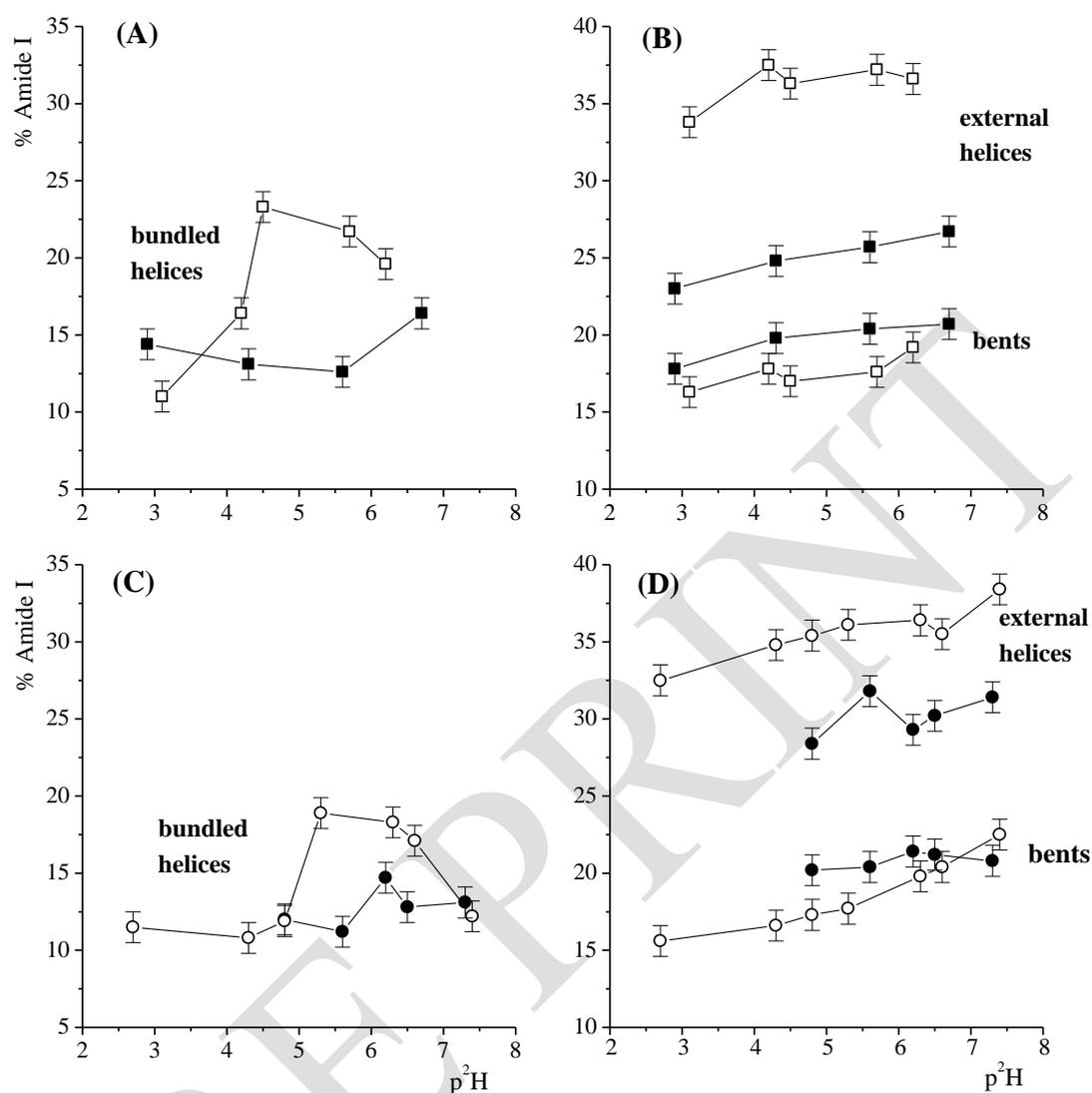
**Figure 6.** Evolution of the Amide I components (%) for BSA secondary structures at various p$^2$H, at t = 2 h. BSA in solution at 30 g. L$^{-1}$ —∅—, or adsorbed on montmorillonite —■— (A, B); BSA in solution at 4 g. L$^{-1}$ —o—, or adsorbed on talc —●— (C, D).

**Figure 7.** Evolution of the Amide I components (%) for BSA random structures at various

$p^2H$, at t = 2 h. BSA in solution at 30 g. $L^{-1}$ —⌀—, or adsorbed on montmorillonite —■— (A,

B); BSA in solution at 4 g. $L^{-1}$ —○—, or adsorbed on talc —●— (C, D).